doi:10.1016/j.jmb.2005.09.031 J. Mol. Biol. (2005) 354, 272–288

JMB

Available online at www.sciencedirect.com

SCIENCE DIRECT®

ELSEVIER

Electrostatics of the Intracellular Vestibule of K^+ Channels

Vishwanath Jogini and Benoît Roux*

Department of Physiology & Biophysics, Weill Medical College of Cornell University 1300 York Avenue, New York NY 10021, USA

Previous calculations using continuum electrostatic calculations showed that a fully hydrated monovalent cation is electrostatically stabilized at the center of the cavity of the KcsA potassium channel. Further analysis demonstrated that this cavity stabilization was controlled by a balance between the unfavorable reaction field due to the finite size of the cavity and the favorable electrostatic field arising from the pore helices. In the present study, continuum electrostatic calculations are used to investigate how the stability of an ion in the intracellular vestibular cavity common to known potassium channels is affected as the inner channel gate opens and the cavity becomes larger and contiguous with the intracellular solution. The X-ray structure of the calcium-activated potassium channel MthK, which was crystallized in the open state, is used to construct models of the KcsA channel in the open state. It is found that, as the channel opens, the barrier at the helix bundle crossing decreases to ≈ 0 kcal/mol, but that the ion in the cavity is also significantly destabilized. The results are compared and contrasted with additional calculations performed on the KvAP (voltage-activated) and KirBac1.1 (inward rectifier) channels, as well as models of the pore domain of Shaker in the open and closed state. In conclusion, electrostatic factors give rise to energetic constraints on ion permeation that have important functional consequences on the various K^+ channels, and partly explain the presence or absence of charged residues near the inner vestibular entry.

*Corresponding author

Keywords: KcsA; MthK; KirBac1.1; KvAP; Shaker

Introduction

Potassium channels are tetrameric membrane-spanning proteins that serve to facilitate and control the passage of K ions across the lipid membrane.[1] The determination of the structure of the KcsA K^+ channel by X-ray crystallography provided the first atomic-resolution view of these proteins.[2] The most important functional feature of the channel structure, shown in Figure 1, is the 12 Å long narrow pore located along the tetrameric symmetry axis near the extracellular side. Lined exclusively by main-chain carbonyl oxygen atoms from the residues corresponding to the signature sequence TTVGYG common to all K^+ channel,[3] this region of the protein acts as a "selectivity filter" by allowing only the passage of nearly dehydrated K ions. Short α-helices from each of the four subunits, referred to as the pore helices, surround the selectivity filter with their COOH termini pointing toward the center of a wide aqueous cavity, about 15 Å in diameter and able to contain 25 to 30 water molecules. It has been suggested that this aqueous cavity, located at the center of the membrane, helps overcome the electrostatic barrier to ion translocation that is opposed by the low dielectric membrane lipid.[2] Common monovalent cations have indeed been observed occupying the cavity in the crystallographic structure,[4] and continuum electrostatic calculations have shown that the static and reaction fields in the channel are tuned to exclusively stabilize a monovalent cation at the center of the cavity of the KcsA channel, thus revealing that the channel has the ability to exert a crude form of valence selectivity while keeping incoming cations

Abbreviations used: MD, molecular dynamics; ESR, electron spin resonance; PB, Poisson–Boltzmann; ABNR, adopted basis Newton–Raphson; RMSD, root-mean-square-deviation.

E-mail address of the corresponding author: benoit.roux@med.cornell.edu

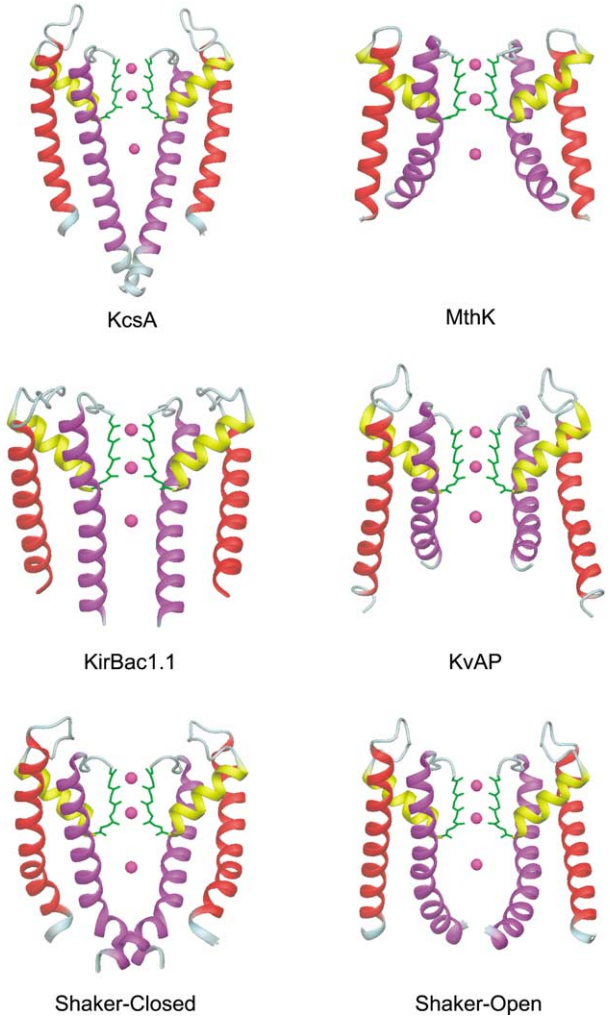

Figure 1. All available K^+ channels. The extracellular side is at the top, and the intracellular side is at the bottom. The main structural elements are the outer helix, the pore helix, the selectivity filter and the inner helix. There are three K ions, two of them are located at S1and S3 position in selectivity filter and one is at the center of the cavity. The Figures were produced with DINO (www.dino3d.org).

fully hydrated.[5] The free energy of a monovalent cation in the cavity was found to result from a balance of two opposing effects: an unfavorable reaction field due to the finite-size of the water-filled high dielectric cavity, and a favorable electrostatic field arising from the charge distribution of the pore helices. Similar α-helices, "interrupted" mid-way through the membrane, are also observed in the case of aquaporins[6] and bacterial ClC homologs,[7,8] and appear to be a recurrent structural motif of membrane channels with an important functional role.

The structure of the KcsA channel, as it appears in the crystal structure, corresponds most likely to a closed state. On the intracellular side, the inner helices from the four subunits cross into a tight bundle of hydrophobic residues, leaving only a narrow entryway of about 4 Å radius to the central cavity. Molecular dynamics (MD) simulations of KcsA in a lipid bilayer indicated that the packing of the inner helices at the bundle crossing is very stable.[9] The passage of a cation through this narrow entrance, which comprises exclusively hydrophobic side-chains, is not sterically disallowed but requires a nearly complete dehydration and is energetically prohibitive.[10] According to continuum electrostatic calculations, increasing the diameter of the inner entrance by only 3 Å is enough to reduce the large entry barrier from 20 to about 3–4 kcal/mol, suggesting that small movements of the inner helices could significantly affect the free energy barrier for ion entrance; effectively closing or opening the channel.[10] This is consistent with available experimental information. In bilayer experiments, the KcsA channel is observed to be mostly closed at neutral pH, and that the probability of channel opening increases up to 5–10% at low intracellular pH.[11–13] Thus, the fact that the KcsA channel was crystallized at pH 5–5.6[14] makes it even more plausible that the X-ray structure corresponds to a closed state.

The X-ray structure of the calcium-activated potassium channel from *Methanobacterium thermoautotrophicum* (MthK), crystallized presumably in an open state with high calcium concentration, revealed the conformational changes associated with channel opening.[15] In the structure of the MthK channel shown in Figure 1, the inner helices are sharply bent away from the central axis at a conserved glycine residue, leaving a wide open entrance to the pore on the intracellular side. Accordingly, the central cavity, which is closed in the case of the KcsA channel, is transformed into a wide vestibular opening that is contiguous with the intracellular side. Data from electron spin resonance (ESR) on KcsA show that the inner helices from the four subunits are moving apart during the conformational change triggered by intracellular pH,[12,16] in a manner that is generally consistent with the X-ray structure of the MthK channel. Furthermore, site-directed mass tagging experiments confirm that the inner helices of KcsA in the open state are a gating component.[17] Crystallographic structures of additional K^+ channels, shown in Figure 1, provide complementary information about the putative open and closed conformation of the pore domain and support the general conclusions drawn from KcsA and MthK. The conformation of the inwardly rectifying K^+ channel (KirBac1.1) from *Burkholderia pseudomallei*[18] is very similar to that of the closed KcsA structure, whereas the conformation of the pore domain of the voltage-activated K^+ channel (KvAP) from the thermophilic archaebacteria *Aeropyrum pernix*[19] resembles that of the open MthK structure. In the case of the KvAP channel, the extensive distortion in the voltage sensor[19] casts some doubts on the validity of the conformation of the pore domain, though the structure is very useful because it provides one more example of a channel that is possibly in an open state.

There is also evidence that the main features of the intracellular gate formed by the inner helices can be found in eukaryotic channels. Based on electrophysiological experiments on the BK channel (large conductance calcium-activated potassium channel), Aldrich *et al.*,[20] suggested that the conformation adopted by the inner helix in the open state determines the extent of access resistance on the ion permeation pathway. They concluded that large conductance channels such as BK and KcsA might adopt the wide-open conformation. The voltage-gated Shaker channel has a PVP motif in the inner helix, which suggests that its open state may differ from that of MthK. Based on cysteine accessibility to chemical modification, Yellen and co-workers[21–23] suggested that the gating in Shaker is accompanied by the movement of inner helices. They concluded that the architecture of Shaker in its closed state is similar to that of KcsA, except for a bend in the inner helix (Figure 1). They could also stabilize a mutant of Shaker in the open state (V476C) using cadmium-binding experiments by bridging the cysteine at position 476 to the histidine at position 486 in an adjacent subunit; though Bruhova & Zhorov have suggested that the resulting distance constraint between Cys476 and His486 may not be interpreted in terms of a unique open channel conformation.[24] Very recently, the structure of the eukaryotic voltage-activated Kv1.2 channel has been determined.[25] Comparison with the pore domain of the bacterial KvAP channel shows that the latter constitutes a good template for modeling the open state of Kv channels.

Although the fine details of the molecular processes associated with gating are probably not universal for all K^+ channels, it seems clear that controlling the size of the aperture at the helical bundle crossing on the intracellular side by bending the inner helices is an important mechanism. Previous calculations using continuum electrostatic showed that the electrostatic field from the pore helices contribute significantly to stabilize a monovalent cation inside the aqueous cavity of the closed KcsA channel.[5] Important questions arise concerning the electrostatic stabilization of a cation and how it is going to be affected when the channel opens up and the geometry of the inner entrance, with all its complex dielectric boundaries, is altered. The goal of the present study is to characterize the electrostatic properties of the channel in the open state and see how they relate to those of the channel in the closed state. The approach that we take consists in determining the free energy to transfer a cation from the bulk to the channel environment using computations based on the finite-difference Poisson–Boltzmann (PB) equation.[5,10,26] The influence of the pore architecture and amino acid sequence on the ion in the intracellular vestibule is analyzed using all the available X-ray structures as well as models of K^+ channels. The paper is concluded with a discussion of the possible biological implications of the main findings.

Theory and Methods

Decomposition of the electrostatic free energy

The electrostatic free energy to transfer an ion from the bulk solution to a point $\mathbf{r}$ in the pore can be calculated as the difference between the electrostatic free energy of the ion-channel complex (ic) and, the free energy of the isolated channel (c) and ion (i) in water:

$$\Delta\Delta G(\mathbf{r}) = [\Delta G^{\mathrm{ic}}(\mathbf{r}) - \Delta G^{\mathrm{c}} - \Delta G^{\mathrm{i}}] \tag{1}$$

where $\Delta G^{\mathrm{ic}}(\mathbf{r})$ is the electrostatic energy of the channel with the ion at $\mathbf{r}$, ΔG^{c} is the electrostatic energy of the channel in the absence of the ion at $\mathbf{r}$, and ΔG^{i} is the electrostatic energy of the K ion far away in bulk water. Each ΔG is calculated as a sum over all the atomic charge q_{i} of the protein and ions present in the system:

$$\Delta G = \frac{1}{2}\sum_i q_i \phi(\mathbf{r}_i) \tag{2}$$

where $\phi(\mathbf{r}_i)$ is the electrostatic potential at the position of the atomic charge q_i. It is calculated by solving the PB equation:[27,28]

$$\nabla\cdot[\epsilon(\mathbf{r})\nabla\phi(\mathbf{r})] - \bar{\kappa}^2(\mathbf{r})\phi(\mathbf{r}) = -4\pi\rho(\mathbf{r}) \tag{3}$$

where $\rho(\mathbf{r}) = \sum_i q_i\delta(\mathbf{r}-\mathbf{r}_i)$ is the total atomic charge distribution in the system, $\epsilon(\mathbf{r})$ is the position-dependent dielectric constant, and $\bar{\kappa}(\mathbf{r})$ is the position-dependent ionic screening constant (it is 0 for present calculations). In practice, the $\mathbf{r}$-dependent functions $\rho(\mathbf{r})$, $\epsilon(\mathbf{r})$ and $\bar{\kappa}(\mathbf{r})$ are mapped onto a cubic discrete grid and the potential $\phi(\mathbf{r})$ is calculated by solving the PB equation with a finite-difference method.[28]

The total electrostatic free energy in equation (2) can be formally expressed using the Green's function M for the complex (ic), isolated channel (c) and ion (i).[29] For the sake of simplicity, let us assume that the ion is particle $i=1$ carrying a charge q_1. The free energy of the complex is then:

$$\begin{aligned}
\Delta G^{\mathrm{ic}} &= \frac{1}{2}\sum_{i=1,j=1}^{n} q_i M^{\mathrm{ic}}(i,j) q_j \\
&= \frac{1}{2} q_1 M^{\mathrm{ic}}(1,1) q_1 + \frac{1}{2}\sum_{j=2}^{n} q_1 M^{\mathrm{ic}}(1,j) q_j \\
&\quad + \frac{1}{2}\sum_{i=2}^{n} q_i M^{\mathrm{ic}}(i,1) q_1 + \frac{1}{2}\sum_{i=2,j=2}^{n} q_i M^{\mathrm{ic}}(i,j) q_j \\
&= \frac{1}{2} q_1 M^{\mathrm{ic}}(1,1) q_1 + \sum_{j=2}^{n} q_1 M^{\mathrm{ic}}(1,j) q_j \\
&\quad + \frac{1}{2}\sum_{i=2,j=2}^{n} q_i M^{\mathrm{ic}}(i,j) q_j
\end{aligned} \tag{4}$$

(the symmetry property of the Green's function

$M^{ic}(i,j)=M^{ic}(j,i)$ has been used). The free energy of the isolated protein can be expressed as:

$$\Delta G^{c} = \frac{1}{2}\sum_{i=2,j=2}^{n} q_i M^{c}(i,j) q_j \tag{5}$$

and the free energy of the isolated ion in solution can be expressed as:

$$\Delta G^{i} = \frac{1}{2} q_1 M^{i}(1,1) q_1 \tag{6}$$

The general solution for the electrostatic free energy for transferring the charge q_1 from the bulk to an inhomogeneous medium with dielectric boundaries having both reaction field and static field terms may be expressed as:

$$\begin{aligned}\Delta\Delta G &= [\Delta G^{ic} - \Delta G^{c} - \Delta G^{i}] \\ &= \frac{1}{2} q_1 M^{ic}(1,1) q_1 + \sum_{j=2}^{n} q_1 M^{ic}(1,j) q_j \\ &\quad + \frac{1}{2}\sum_{i=2,j=2}^{n} q_i M^{ic}(i,j) q_j - \frac{1}{2} q_1 M^{i}(1,1) q_1 \\ &\quad - \frac{1}{2}\sum_{i=2,j=2}^{n} q_i M^{c}(i,j) q_j\end{aligned} \tag{7}$$

and:

$$\begin{aligned}\Delta\Delta G &= \frac{1}{2} q_1 [M^{ic}(1,1) - M^{i}(1,1)] q_1 \\ &\quad + q_1 \left[\sum_{j=2}^{n} M^{ic}(1,j) q_j\right] \\ &\quad + \left[\frac{1}{2}\sum_{i=2,j=2}^{n} q_i [M^{ic}(i,j) - M^{c}(i,j)] q_j\right]\end{aligned} \tag{8}$$

which can be written as:[5]

$$\Delta\Delta G = \frac{1}{2} q_1^2 A + q_1 B + C \tag{9}$$

where A corresponds to the magnitude of the reaction field contribution, B to the magnitude of the static field contribution, and C is a constant term due to the influence of the dielectric constant of the ion on the protein charges. The constant A depends on the geometry and the size of the high dielectric aqueous cavity. The constant B depends on the electric field arising from the static charge distribution on channel shielded by the dielectric regions. In the case of a small ion, the constant C is normally negligible ($\simeq$0.2 kcal/mol) and the free energy of an ion in the pore calculated from the PB equation is typically dominated by the contributions from static and reaction field.[5,10,29] (note that C is exceptionally equal to 2.5 kcal/mol in the case of the open state model I of KcsA because the presence of the ion inside the cavity creates a region of low dielectric constant that gives rise to an unfavorable dehydration of Thr75).

A special procedure was designed to efficiently dissect all the contributions to the total electrostatic free energy of an ion along the channel axis. According to equation (9), the total free energy is dominated by the reaction field ΔG^{rf} and the static field ΔG^{sf} contributions. The reaction field contribution is calculated using $\Delta G^{rf}=[\Delta G^{ic}-\Delta G^{i}]$. This can be calculated using a single PB calculation in which the protein charge have been turned off to zero followed by a reference PB calculation corresponding to the isolated ion in the bulk. The static field contribution is a linear sum of the static field from each charges of the protein:

$$\begin{aligned}\Delta G^{sf} &= \sum_{j=2}^{N} q_1 M^{ic}(1,j) q_j \\ &= q_1 \phi^{ic}(\mathbf{r}; q_1 = 0, q_2, \ldots, q_N)\end{aligned} \tag{10}$$

In principle, extracting the static field contribution from each residue is possible by solving the PB equation for the field $\phi^{ic}(\mathbf{r};q_1=0,q_2,\ldots,q_N)$, in which all protein charges are turned off except those of the residue of interest. However, such a procedure is highly inefficient to obtain a full dissection of the static field contribution per residue because it would require a full numerical solution to the PB equation for each specific residue. This can be avoided by exploiting the symmetry of the Green's function, $M^{ic}(1,j)=M^{ic}(j,1)$:

$$\begin{aligned}\Delta G^{sf} &= \sum_{j=2}^{N} q_1 M^{ic}(1,j) q_j \\ &= \sum_{j=2}^{N} \phi^{ic}(\mathbf{r}; q_1, q_2 = 0, \ldots, q_N = 0) q_j\end{aligned} \tag{11}$$

To find the contribution from each specific residue on the stability of ion in the cavity, the electrostatic field $\phi^{ic}(\mathbf{r};q_1,q_2=0,\ldots,q_N=0)$, generated by the ion in the cavity is first calculated with all other charges turned off. Then, the interaction energy between the static field and any specific residue is calculated as a simple sum over all the protein charges q_j (with $j=2,\ldots,N$). Using this method, the contribution from each individual residue of the channel to the total static field can be obtained efficiently using a single PB equation.

Atomic models

In the calculations, all the channel atoms and the bound ions (two in the selectivity filter and one in the vestibular cavity) are represented explicitly, with associated atomic charges and radii. The crystallographic structures of the KcsA channel (PDB entry 1BL8 and 1K4C),[2,14] the MthK channel (PDB entry 1LNQ),[15] the pore domain of the KvAP channel (PDB entry 1ORQ),[19] the KirBac1.1 channel

(PDB entry 1P7B)[18] were used. As this study was completed, the structure of the eukaryotic voltage-activated Kv1.2 channel (PDB entry 2A79) was reported.[25] Comparison with the two TM helices of the pore domain S5-S6 of the bacterial KvAP channel shows relatively small differences, with only 2.5 Å RMS deviation for the C atoms and an intracellular opening of about 12 Å radius. This shows that the pore domain of KvAP constitutes a good template for modeling the pore domain of Kv channels in the open state. Missing hydrogen atoms were added using HBUILD within the CHARMM package.[30] In all these structures, the default protonation state was used for all ionizable residues except for Glu71 in KcsA and Glu106 in KirBac1.1 (equivalent to Glu71 in KcsA), which are protonated.[10,31]

An open state model of KcsA was derived from the X-ray structure of the MthK channel (KcsA model I). To obtain a structural alignment, the backbone atoms of the pore helix and selectivity filter of the KcsA channel (residues 60–81) were superimposed onto the corresponding atoms of the MthK channel using the "COOR ORIENT RMS" command of CHARMM.[30] The backbone coordinates of residues 19–31 in the outer helix (TM1) and residues 68–98 in the inner helix (TM2) of the MthK channel were copied to map the position of residues 28–40 (TM1) and 84–114 (TM2), respectively, in the model open state of the KcsA channel. The side-chain were then reconstructed in the same rotameric states as in the high resolution X-ray structure of KcsA (closed state). The model was further relaxed and optimized using adopted basis Newton–Raphson (ABNR) energy minimization in the presence of harmonic restraining potentials used to maintain the secondary structure of the MthK channel. The final model has the same side-chain rotamers as in the closed state KcsA, but the backbone conformation of MthK for the TM1 and TM2 helices. A model of KcsA in the open state based on the KvAP structure was also constructed according to the same procedure (KcsA model II).

Additional intermediate models of KcsA were also generated by interpolating the backbone dihedral angle values between the two end-points closed and open states. The dihedral angles required for generating intermediate structures were calculated as a linear interpolation from closed state to open state (model I). Residues 23–45 in outer helix (TM1) and residues 95–108 in inner helix (TM2) of closed and the modeled open state have very different backbone dihedral values. The backbone dihedrals of these residues are changed to get the intermediate states. The side-chain rotamers were unchanged. The intermediate structures were refined using energy minimization, fixing the invariant parts of the protein.

Lastly, models of the closed and open state of Shaker were examined to broaden the scope of the present study. The model of the closed state, based on residue accessibility,[21–23] was kindly provided by Gary Yellen. The model of the open state of Shaker was constructed following the results of Bruhova & Zhorov.[24] It was derived from the structure of the KvAP channel based on two key observations: (1) Cd^{2+} locks the mutant V476C in the open state by bridging the cysteine at position 476 to the histidine at position 486 from the adjacent helix; (2) Cd^{2+} blocks the locked-open double mutant V474C/V476C by binding to the cysteine at position 474. Both models of Shaker were refined by using SCWRL 2.95[32] followed by energy minimization.

PB computations

All the channel structures are oriented with their pore along the *Z*-axis relative to the membrane (which extends in the *XY* plan). The negative *Z*-axis corresponds to the intracellular side and the positive *Z*-axis corresponds to the extracellular side. The center of the channel cavity is at $Z=0$ Å, located at the center of the membrane spanning from 12.5 Å to −12.5 Å. The aqueous solution (including the water-filled cavity at the center of the channel) is represented as a uniform continuum media with dielectric constant of 80. The channel with all explicit atoms is embedded into a low dielectric planar slab representing the membrane. The hydrocarbon core of the membrane is represented as a uniform slab of 25 Å thickness with a dielectric constant of 2.[33] A value of 2 was assumed for the dielectric constant of the protein interior. A water probe of 1.4 Å radius was used to define the molecular surface corresponding to the dielectric boundary.[29] To insure that the proper dielectric constant is assigned to the interior of the pore and the inner vestibule of the channel, a cylinder of radius r and $\epsilon=80$ is first cut-out from the membrane slab before the channel structure is overlaid onto it (the precise value of the radius is unimportant, as long as the edge of the cylindrical cut is covered by the protein structure). A radius of 8 Å was used for the closed state KcsA and Shaker, 8.5 Å for the KirBac1.1, 15 Å for the open state KcsA and MthK, 12 Å for KvAP and the open state Shaker.

All the PB calculations were performed in two steps with a cubic grid of 130^3 points, starting with a grid spacing of 1.0 Å (with periodic boundary conditions applied in the membrane *XY* plane), followed by a focusing around the main region with a grid spacing of 0.5 Å. All the calculations were performed using the PBEQ module,[29,34,35] which is implemented into the biomolecular simulation program CHARMM.[30] The atomic charges were taken from the all-atom PARAM22 force field[36] of the CHARMM program. The atomic radii used to define the protein–solvent dielectric boundary were optimized to reproduce the results of MD free energy perturbation calculations with explicit water molecules for the 20 standard amino acids.[34]

The representation of the protein interior in terms of a dielectric constant is not unique and has often been the object of detailed discussion.[27,37,38]

Table 1. Total electrostatic free energy (in kcal/mol)

Dielectric constant	Static field energy	Reaction field energy	Total energy
2	−18.8	13.0	−5.6
3	−11.7	8.9	−2.7
4	−8.1	6.8	−1.2
5	−5.9	5.5	−0.3

K ions are kept at the center of the cavity and in the S1 and S3 positions in the selectivity filter.

Using Frohlich–Kirkwood theory of dielectrics, it was shown that the dielectric constant of the hydrophobic core of protein is small (2 to 5), much larger for surface regions containing charged side-chains (20–35), and intermediate values for the active sites of enzyme (≈10).[37–39] As pointed out by Warshel, the effective dielectric constant attributed to the protein region depends on what atoms are treated explicitly and which thermal motions are "averaged out".[38,40] In our calculations, all the protein atoms are included explicitly and no induced dipoles are present. To assess the importance of the protein dielectric constant, the stability of a K^+ in the cavity was calculated using a dielectric constant for the protein ranging from 2 to 5. The results are given in Table 1. The free energy to transfer a K^+ from the bulk to the center of the cavity, with all protein charges set to zero, depends weakly on the protein dielectric constant for values ranging from 2 to 5. For a dielectric constant of 2, the ion in the cavity display maximum stability (−5.6 kcal/mol). In comparison, the result of MD free energy perturbation calculations with explicit water molecules indicates that the stability of the ion in the cavity is roughly −2.2 kcal/mol. A protein dielectric constant of 2 or 3 yields a similar stability. To be consistent with our previous studies, the protein dielectric constant was set to 2 in the present calculations.

The protonation state of Glu130 in KirBac1.1, a residue close to the cavity region, was examined using continuum electrostatic calculations. The shift in pK_a (ΔpK_a) is expressed relative to the intrinsic pK_a of the amino acid isolated in solution by considering the free energy of transfer $\Delta\Delta G$ that corresponds to the reversible work needed to protonate the side-chain in the protein compared to the work needed to protonate the same side-chain in an isolated peptide in bulk water.[41,42] This free energy difference is converted in terms of ΔpK_a as follows:

$$\Delta pK_a = -\frac{\Delta\Delta G}{2.3k_B T} \tag{12}$$

where $\Delta\Delta G$ is the free energy difference between the protonated (p) and the unprotonated (u) states of an amino acid embedded in protein in reference to the difference for the isolated amino acid in solution:

$$\Delta\Delta G = [\Delta G_{\text{protein}}(\text{p}) - \Delta G_{\text{protein}}(\text{u}) - \Delta G_{\text{isolated}}(\text{p}) + \Delta G_{\text{isolated}}(\text{u})] \tag{13}$$

Results and Discussion

The alignment of the amino acid sequence of all K^+ channels considered in the present study is shown in Figure 2. All those channels display a high sequence similarity and are expected to share the same basic tetrameric pore-forming domain topology as that of the crystallographic structures of the four bacterial channels that are currently available: KcsA, MthK, KirBac1.1, and KvAP (Figure 1). In all the structures, the pore helices point toward the center of the cavity (though there is a slight changes in the orientation of the pore helix in KirBac1.1).

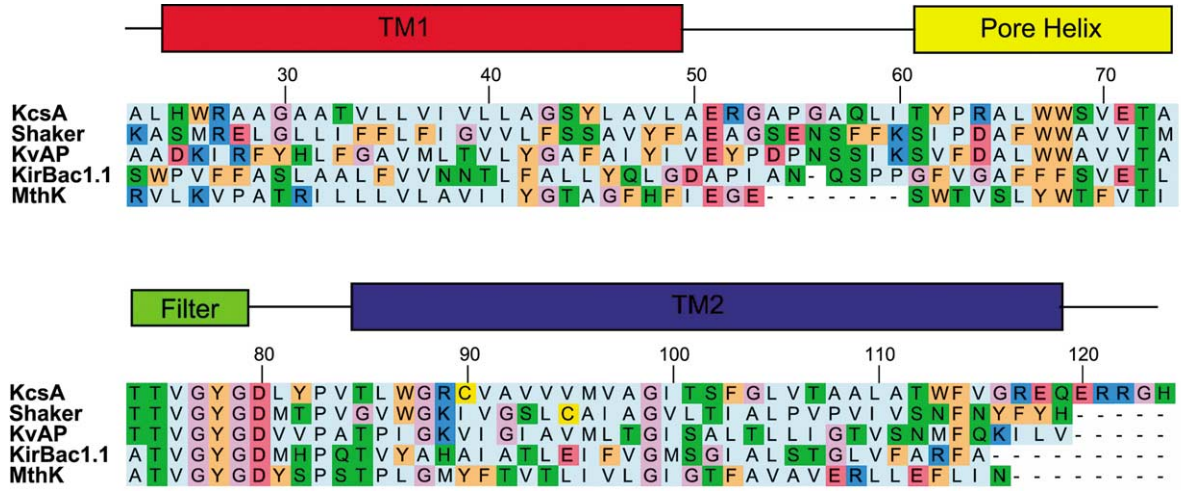

Figure 2. Multiple sequence alignment of different members of K^+ channel family. The general topology of the pore domain of K^+ channels is indicated at the top (inner helix or TM1, outer helix or TM2, pore helix, and selectivity filter). The sequence alignment was generated with CLUSTAL W[52] and edited with Jalview (www.jalview.org).

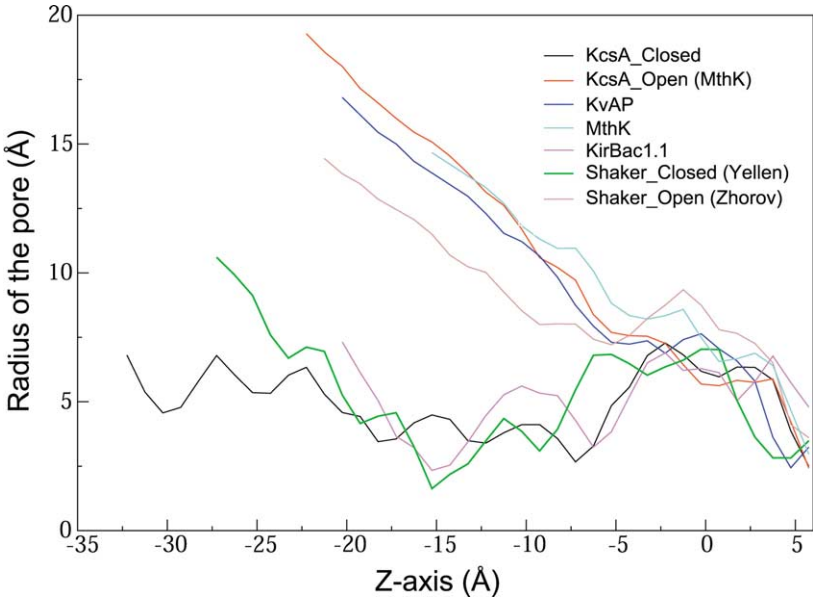

Figure 3. Channel pore radii versus position along the channel axis. The closed state of KcsA extends up to 30 Å and all other channels are short (20–25 Å).

The conformation of the inner helix (TM2) varies significantly, and this has an important impact on the width of the intracellular entrance, as revealed by the radius of the pore along the central axis shown in Figure 3. There is a narrow pore entrance on the intracellular side for the KcsA and KirBac1.1 (X-ray structures 1K4C and 1P7B), which correspond (presumably) to closed state channels. In contrast, the pore entrance is much wider for the MthK and the KvAP, which correspond (presumably) to open state channels. Hence, it may be expected that important differences in the electrostatic properties will occur as a result of changes in the three-dimensional protein structure. Furthermore, the amino acid sequence could also have an important impact on the electrostatic properties. It is of interest to eliminate the influence of sequence variations to isolate the differences in electrostatic properties caused by the structural changes. To this end, models of KcsA in putative open states constructed on the basis of the X-ray structure of the MthK and KvAP channels were included in the analysis. Models of the voltage-gated Shaker channel, which has been extensively studied despite the lack of atomic resolution structure, were also included for the sake of completeness.

Although the radius of the lumen of the pore shown in Figure 3. can be informative, microscopic factors having an impact on ion permeation are revealed more directly by considering the total free energy profile of an incoming ion along the channel axis. This comprises the van der Waals interaction energy between the ion and the channel, and the electrostatic free energy. Slight variations in pore

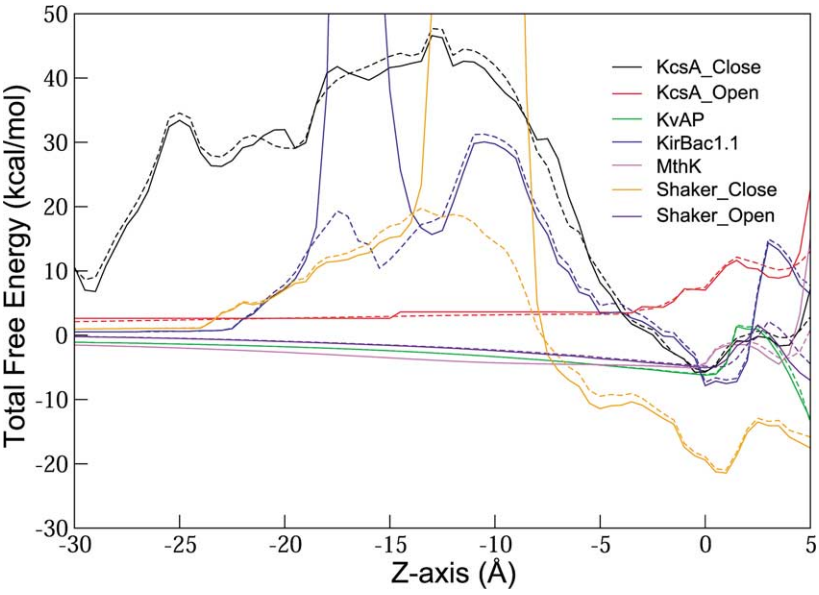

Figure 4. Free energy profile of an ion transferring from bulk to the center of the cavity in all available K^+ channels. In these channels two K ions are placed at S1 and S3 position in the selectivity filter. The broken line represents just electrostatic energy. The continuous line represents the total transfer free energy after inclusion of the van der Waals interaction between the cation and the channel.

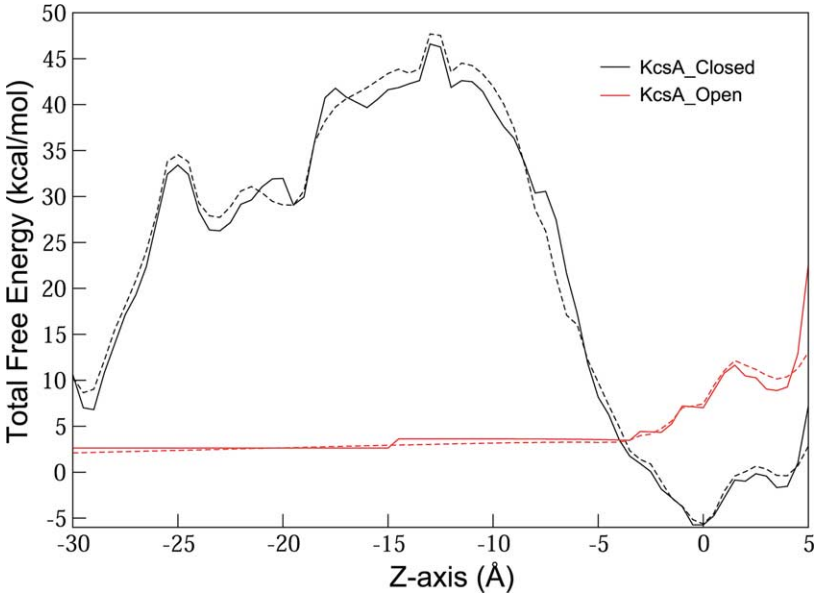

Figure 5. Free energy profile of an ion transferring from the bulk into the pore of the KcsA channel for the closed (X-ray) and the open state (model I). Two K ions are located in the S1 and S3 binding sites in the selectivity filter. The broken line represents just electrostatic energy. The continous line represents the total transfer free energy after inclusion of the van der Waals interaction between the cation and the channel.

radius can give rise to large differences in van der Waals interactions. For example, there exists a large energy barrier in the inner vestibule of KirBac1.1 because there is a steric clash between the ion and Phe139, which essentially occludes the pore (Figure 4). Similarly, there is a large barrier arising from a clash with Val478 in the model of the closed state of Shaker. In contrast, no significant steric clash is opposing the passage of a probe ion through the narrow entrance of the KcsA channel (there is no steric clash until the ion approaches the selectivity filter as seen in Figure 4 and repeated in Figure 5 for the sake of clarity). Nonetheless, it is not necessary to completely occlude the pore entrance to create a large energy barrier opposing the passage of an ion through the narrow non-polar entrance for the KcsA channel in a closed state. As shown in Figure 6, the barrier results from the reaction field energy which corresponds essentially to a dehydration penalty. Similar observations have been made for other model pores.[43]

Effect of opening the intracellular gate

In order to highlight the electrostatic properties arising purely from the structural aspects corresponding to the opening of the intracellular gate formed by the inner helix bundle crossing, it is necessary to eliminate the possible variations caused by differences in amino acid sequence. For this purpose, the KcsA sequence was mapped onto the MthK (open state) structure. Although there is significant uncertainty about the magnitude of the movement of the inner helices in KcsA gating,[12,17,44]

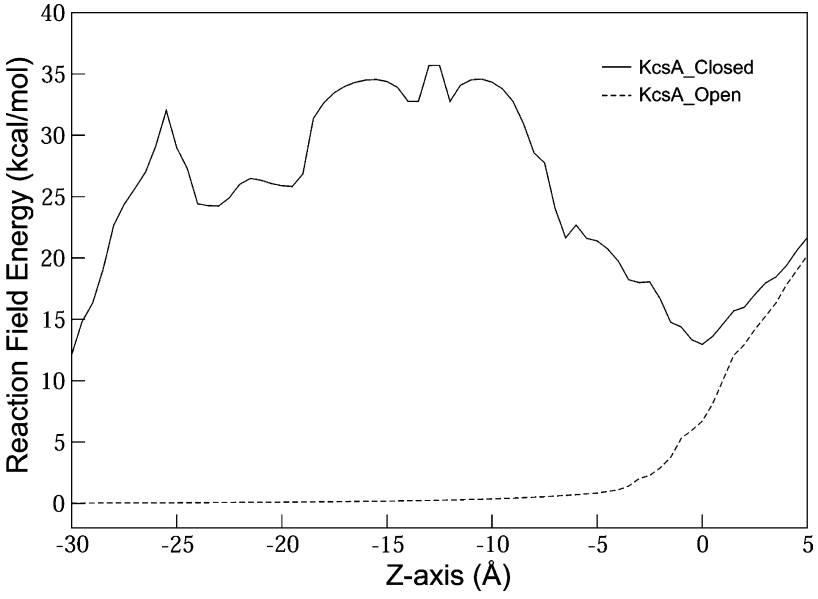

Figure 6. Reaction field contribution to the electrostatic energy profile through the intracellular entrance of KcsA. All charges (other than that of the probe cation) have been turned off.

the similarity between MthK and KcsA (particularly with the conserved glycine "hinge" in TM2) is sufficient to make this model meaningful. To further explore the importance of the width of the intracellular gate, additional models falling between the closed and open end-states were also generated and analyzed using continuum electrostatic calculations These intermediate models were constructed using a simple linear interpolation scheme of the backbone dihedral angles of the residues on TM1 and TM2 (see Theory and Methods). In the model with maximum opening, the width of the vestibular entry is about 15 Å in diameter and the central cavity of the pore becomes contiguous with the intracellular solution. Accordingly, the dielectric interfaces in the closed and the open state of KcsA K^+ channel differ extensively. These significant changes are expected to affect the stability of the ion in the cavity. The electrostatic reaction field profile of the open and the closed state of KcsA through the inner mouth is shown in Figure 6. It is observed that an ion going through the narrow inner entrance of the closed state experiences a very large energy barrier due to electrostatic reaction field.[10] The large energy barrier in the closed state KcsA K^+ channel can be attributed to the inner helix crossing at $Z = -18$ Å to $Z = -13$ Å. In the open state, the diameter of the pore on the inner side is larger and the energy barrier at the intracellular entrance is reduced to ≈ 0 kcal/mol. Perhaps more surprisingly, the total electrostatic free energy of transfer of K^+ ion from bulk to the center of the cavity changes from -5.6 kcal/mol for the closed state, to 7.6 kcal/mol for the open state (Figure 5). As expected, the reaction field contribution to the free energy is reduced in the open state relative to the closed state. The reaction field is typically of the order of 11–13 kcal/mol for the closed state and about 2–3 kcal/mol for the open state. Exceptionally, the value for the open state of the KcsA based on MthK (model I) is slightly larger (6.7 kcal/mol) than for other channels in the open state because the width of the vestibular cavity of MthK used as template for model I is actually narrower than that of KcsA (see Figure 3 at $Z \approx 0$). Nonetheless, the overall reduction in reaction field energy does not necessarily lead to a net increase in stability for a cation in the cavity because the static field contribution of the pore helices in stabilizing the cavity ion in the closed state is -27.5 kcal/mol, whereas it is only -7 kcal/mol in the open state. When the channel is open, the cavity becomes more exposed to bulk water, resulting in a high dielectric environment in the vicinity of the cavity ion and the pore helices. As a consequence, the contribution of the pore helices in stabilizing an ion in the cavity is much smaller in the open state than in the closed state. In fact as shown in Figure 7, the static field contribution from all residues is smaller in the open state relative to the closed state. Therefore, despite a decrease in the unfavorable reaction field contribution in the open state, a cation in the cavity is significantly less stable in the open state than the closed state because the static field contribution is extensively reduced.

The backbone charge distribution of the pore helices makes an important contribution to the stability of K ion in the cavity of the closed state of KcsA K^+ channel. The total interaction energy of the pore helices and the cavity ion is -27.5 kcal/mol, which is mostly from the backbone atoms of the pore helix residues. This energy roughly compensates the unfavorable reaction field contribution of $+13$ kcal/mol for the transfer of a cation to the center of the cavity. The results based on the 1K4C X-ray structure of KcsA resolved at 2.0 Å resolution[45] differs slightly from the previous

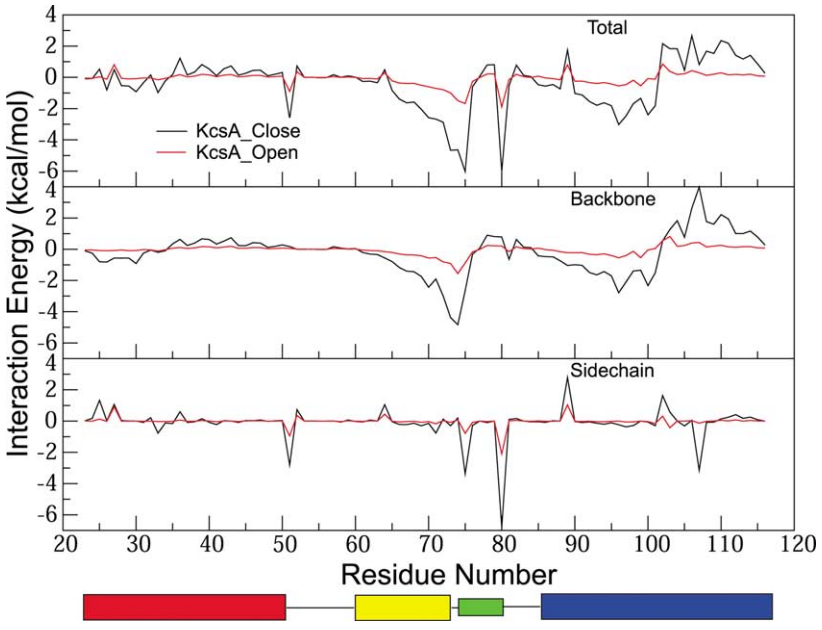

Figure 7. Static field energy where the interaction between the cavity ion and individual residues is calculated for the KcsA closed and open model. The general topology of K^+ channels is given at the bottom of the Figure.

Table 2. Total electrostatic free energy (in kcal/mol)

	1BL8			1K4C		
Environment	Reaction field	Protein	Pore helices	Reaction field	Protein	Pore helices
Membrane	10.7	−8.9	−1.3	13.0	−5.6	−1.7
Bulk water	7.2	−10.5	−0.3	10.7	−6.0	−0.6

In all the calculations ions in the selectivity filter are in S1 and S3. The pore helix consists of residues Tyr62 to Thr74 in addition to the main-chain atoms of Thr75 (excluding carbonyl) and Tyr62 (excluding nitrogen). Protein and Pore helices refer to the part of the protein where charges have been turned on.

Table 3. Total electrostatic free energy (in kcal/mol)

State of KcsA	Structure	Reaction field	Pore helix	TM2N	TM2C	TM2
Closed state	X-ray (1K4C)	13.0	−27.5	−16.6	19.8	3.2
Open state I[a]	Model based on MthK (1LNQ)	6.7	−7.0	−3.2	5.4	2.2
Open state II[b]	Model based on KvAP (1ORQ)	2.4	−7.1	−4.0	5.9	1.9

The reaction field energy of the cavity ion (with entire protein charge and ions in the selectivity filter set to zero) is calculated and multiplied by the total charge of pore helix or TM2N or TM2C.
[a] Modeled on MthK.
[b] Modeled on KvAP.

results,[5] which were obtained from the 1BL8 structure resolved at 3.2 Å.[2] In these early calculations, the dielectric interface was generated simply from the van der Waals surface of the protein (i.e. using an overlapping spheres procedure). The previously calculated free energy of a cation at the center of the cavity of the KcsA channel in the closed state was −8.5 kcal/mol.[5] For comparison, all the calculations are repeated here with a more accurate definition of the dielectric interface based on the regions accessible to a probe with a radius of 1.4 Å, corresponding to the size of a water molecule. The results, given in Table 2, show that the ion in the center of the cavity is stabilized by −8.9 kcal/mol using the 1BL8 structure. However, the stability is apparently reduced to −5.6 kcal/mol with the 1K4C structure. The difference is partly due to the five additional residues at the C-terminal (ERRGH) in the 1K4C structure, corresponding to a net positive charge. These residues contribute to destabilize an ion in the cavity by about 1.5 kcal/mol. The small structural differences between the 1BL8 and 1K4C X-ray structures are at the origin of the remaining difference. These two structures have a root-mean square deviation (RMSD) of 1.77 Å for all non-hydrogen atoms, and 1.0 Å for the C^{α}. For example, the reaction field energy is 11 kcal/mol and 13 kcal/mol for the 1BL8 and 1K4C structures, respectively, due to slight differences in the shape of the dielectric interface of the two structures in the cavity region. This is caused, in particular, by the small difference in the orientation of the large

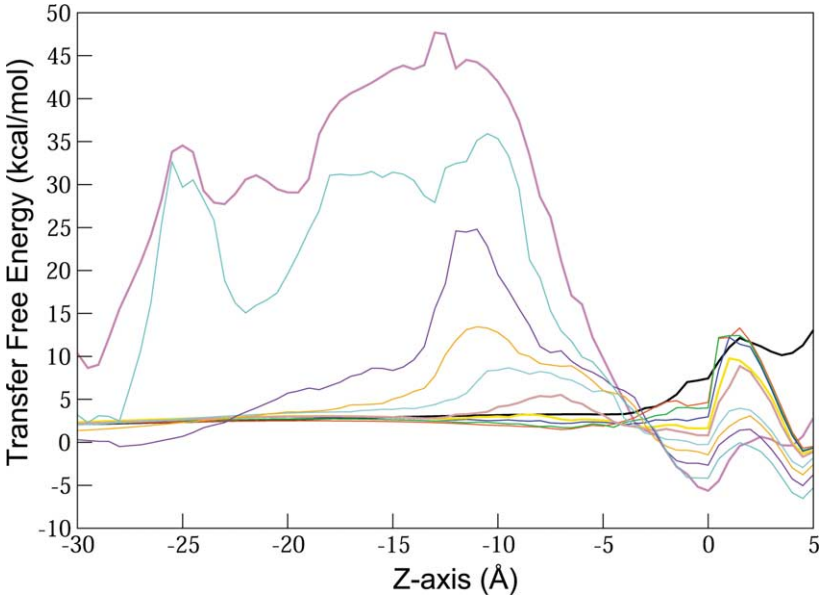

Figure 8. Transfer free energy of an ion from bulk to the channel in all the intermediate structures. The energy profile in the closed state is represented by magenta and in the open state by black color (in bold). The intermediate states which might be the true open state are represented as brown and yellow continous lines.

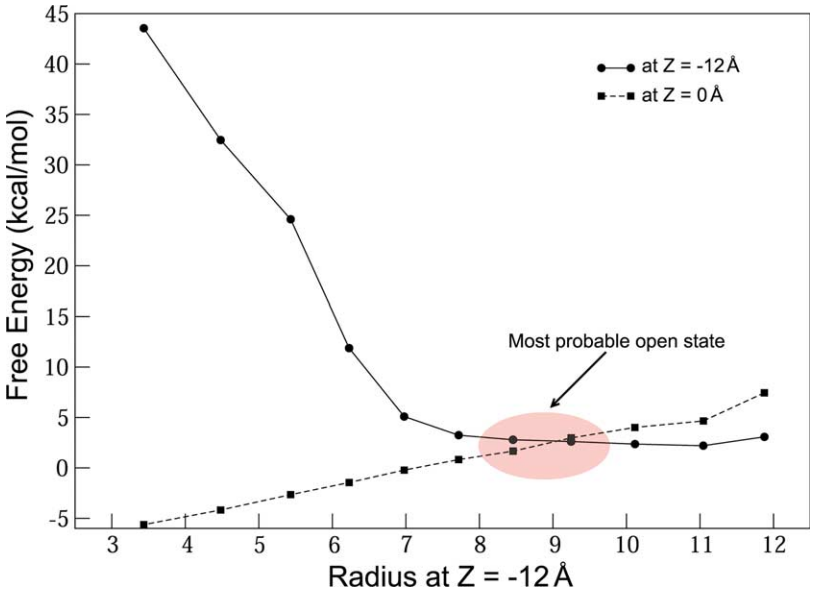

Figure 9. The free energy barrier encountered by a cation at the helical bundle crossing (continous line), and the free energy of a cation at the center of the vestibular cavity (broken line) plotted as a function of the radius of the pore entrance at the helical bundle crossing.

non-polar side-chain of Phe103. Furthermore, a residue-by-residue decomposition of the total electrostatic free energy indicates that Thr75 is the cause of the remaining difference (data not shown). Lastly, there are also small differences arising from backbone and side-chains atoms from other residues (e.g. caused by a small difference in the orientation of Ser102). Such variations in electrostatic free energy caused by small differences in structure show that precise numerical results have a limited significance.

Despite the sensitivity on channel structure, the most important trends are robust and unambiguous. For instance, in both structures of KcsA corresponding to the closed state of KcsA the pore helices contribute nearly 80% to the total stabilization energy of a monovalent cation in the cavity, in accord with previous calculations.[5] The residues nearest to the cavity clearly make the largest contribution (about 60% of the total interaction energy comes from the first turn of the helix), though the contribution from the remaining residues is not negligible. This situation differs qualitatively from that observed in the bacterial ClC channel homolog, where the N termini residues of nearby helices, which are essentially in close contact with the chloride anion, make the dominant contribution.[46] A similar analysis carried out for the C-terminal and N-terminal segments of TM2 (TM2C and TM2N) indicates that the residues nearest to the cavity yield also a large interaction, but with a magnitude that is overall smaller than that of the pore helices. It is the opening of the intracellular entrance to the channel that significantly decreases the contribution from the pore helices. The total stabilization from the pore helices is only -7 kcal/mol in the open state,

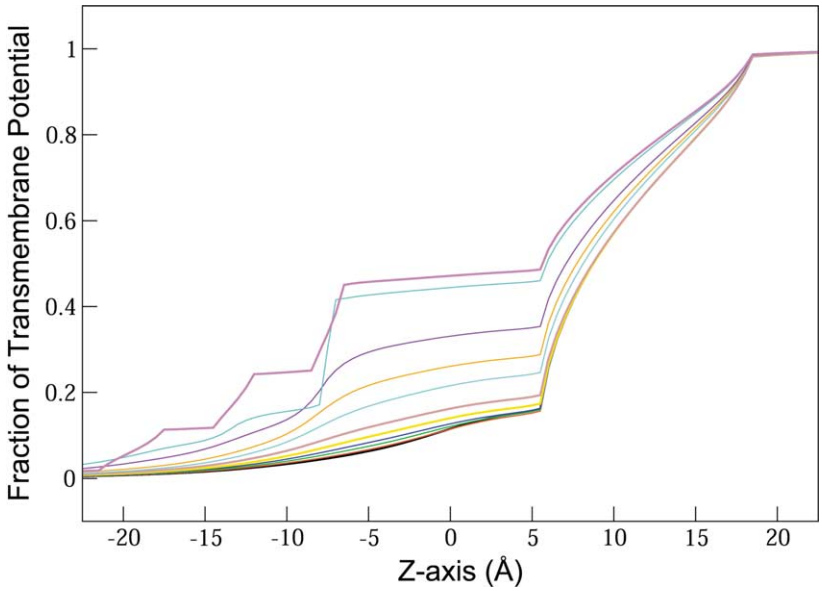

Figure 10. Fraction of transmembrane potential along the axis of all intermediate structures. The curve is drawn relative to extracellular solution which is assumed to have positive unitary value. The closed state is represented by magenta and the open state by black.

compared to −27.5 kcal/mol in the closed state. This static field energy of −7 kcal/mol cannot compensate for the unfavorable reaction field and the additional unfavorable interaction energy coming from positively charged residues near the C terminus of TM2. As shown in Table 3, the helical elements TM2C and TM2N make opposite contributions to the total electrostatic free energy, yielding a destabilization of the cation in the cavity (of about 2 to 3 kcal/mol). As in the case of the pore helix, the total effect is decreased slightly for the open state.

The free energy profiles from the intermediate models shown in Figure 8 fall between the closed and open states. Of particular importance, the stability of a monovalent cation in the center of the cavity increases systematically as the channel is transformed from the open to the closed state. The net energy barrier for the transfer of an ion from bulk to the inner helix bundle crossing decreases as the gate opens. However, the static field contribution from the pore helices and the charged residues is almost negligible in the fully open state. In fact, the energy barrier at the inner helix bundle crossing becomes zero before reaching the fully open state generated from the MthK structure (Figure 8). It was shown previously that an increase in the diameter of the pore by 3 Å at the bundle crossing was sufficient to abolish the entrance energy barrier.[10] As shown in Figure 9, increasing the radius up to 15 Å does not result in further reduction of the barrier opposing ion entry. The analysis of these intermediate states suggests that there is an optimal opening for which there is neither an energy barrier near the entrance of the pore, nor a deep energy well for a cation in the cavity (the states corresponding to the brown and yellow curves in Figure 8, have no entry barrier and the energy of an ion in the cavity is 0.8 kcal/mol to 1.7 kcal/mol). Though additional factors related to diffusion and access resistance should also be taken into consideration, such an open state presenting a flat energy landscape might be expected to yield maximum ion conduction. According to Figure 9, the pore opening needs to be roughly 9 Å, that is, smaller than the opening suggested on the basis of the X-ray structure of the MthK channel. Interestingly, a model of the open state of KcsA based on the X-ray structure of the KvAP channel exhibit an energy profile similar to such "optimal" model (brown and yellow curves in Figure 8).

In a similar fashion, the transmembrane potential profile is also affected by the channel opening. The transmembrane potential profile along the axis of the KcsA channel, calculated using the modified Poisson–Boltzmann equation,[10,35,47] is shown Figure 10. In the closed state, the potential is distributed almost evenly across the pore, whereas in the open state, it is focused across the selectivity filter. In the intermediate models, the variation in the transmembrane potential difference becomes increasingly localized across the selectivity filter as they approach the open state. The intermediate models (shown as brown and yellow solid lines) have similar transmembrane potential profile as the fully open state generated from the MthK channel (black solid line) (Figure 10). As discussed above, this suggest that the ion conduction properties of such intermediate model might be optimal.

Electrostatics of different K^+ channels

In Table 4, the total electrostatics free energy of a cation at the center of the vestibular cavity for the different models is decomposed in terms of the reaction field and static contributions. The static field contribution from each residue is shown in Figures 11 and 12 for models of the closed and open state. All the closed state channels adopt the inverted tepee architecture, with the narrow helical bundle crossing at the intracellular side. As expected, the energy profile of a cation along the axis of KirBac1.1 and the closed model of Shaker display a large energy barrier on the intracellular side, in qualitative agreement with the results obtained with the closed state KcsA channel. In KirBac1.1, the barrier is even larger because there is a steric clash between the ion and Phe139, which completely occludes the entrance to the pore. Similarly, there is also a large van der Waals barrier in the model of the closed state of Shaker due to the presence of Val478. There is no such steric clashes in the case of the KcsA structure, though the pore is probably in a closed state nonetheless. The total electrostatic free energy of transfer of K ion from the bulk to the center of the cavity is −7.3 kcal/mol for the Kirbac1.1 channel, slightly more negative than the value of −5.6 kcal/mol for the closed state of KcsA (Figure 4 and Table 4). As shown in Figure 11, Thr110 (equivalent to Thr75 in KcsA) in KirBac1.1

Table 4. Comparison of total electrostatic free energy for K^+ channels (kcal/mol)

K^+ channels	State	Structure	Reaction field	Static field		Total
				Pore helix	All atoms	
KcsA	Closed	X-ray (1K4C)	13.0	−27.5	−18.8	−5.6
	Open I	Model based on MthK (1LNQ)	6.7	−7.0	−1.8	7.6
	Open II	Model based on KvAP (1ORQ)	2.4	−7.1	−3.9	−1.4
KirBac1.1	Closed	X-ray (1P7B)	17.3	−27.8	−25.0	−7.3
KvAP	Open	X-ray (1ORQ)	1.6	−6.0	−7.9	−6.1
MthK	Open	X-ray (1LNQ)	2.0	−4.4	−6.9	−4.3
Shaker	Closed	Model from Yellen	18.1	−31.4	−39.3	−20.8
	Open	Model from Bruhova & Zhorov[24]	2.2	−8.0	−7.1	−4.9

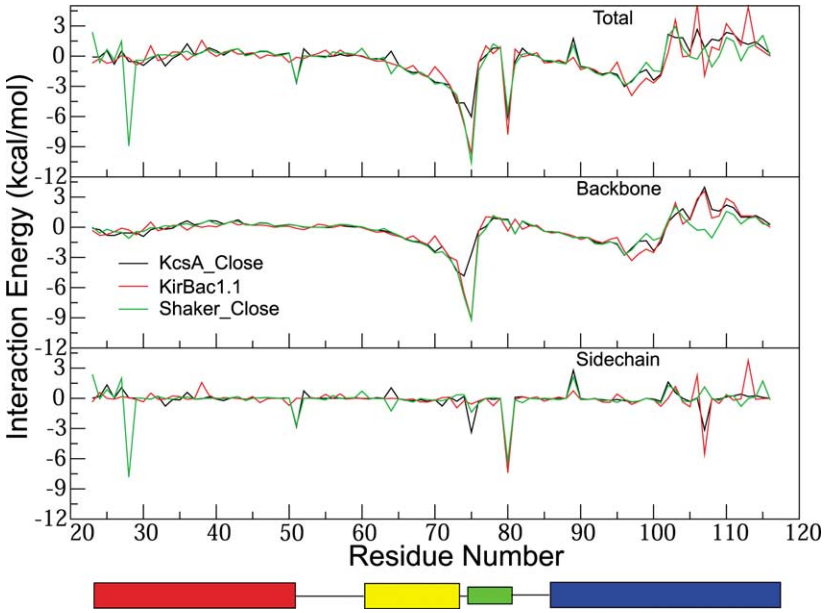

Figure 11. Static field energy where the interaction between the cavity ion and individual residues is calculated for all closed channels. All the channels are aligned according to KcsA (the gaps are assigned a value of zero). The general topology of K^+ channels is given at the bottom of the Figure.

gives rise to a favorable interaction of −3.7 kcal/mol, which accounts partly for the increased stability compared with the closed state of KcsA. Interestingly, unlike in the KcsA channel, the pore helices of KirBac1.1 do not point directly toward the center of the channel cavity. The structural difference has led to the suggestion that the helix dipole effect might be smaller than in KcsA.[18] However, the present calculations indicate that the contribution of the pore helices is essentially the same in KirBac1.1 (−28 kcal/mol) as in the KcsA channel (−27.5 kcal/mol). In both channels, the contribution from the side-chains is almost zero (green line in Figure 11), and the total interaction energy arises almost exclusively from the backbone atoms of the pore helices. The stability of an ion in the cavity of the closed state model of Shaker is −21 kcal/mol, which is noticeably more negative than the corresponding value calculated for the KcsA and KirBac1.1 channels. The increased stability in the case of Shaker can be attributed partly to the pore helices (−31.4 kcal/mol in Table 4), but mostly to the negatively charged residues (Glu395, Glu418) located along the outer and inner helices (see Figures 2 and 11).

The dominant feature of the free energy profile common to all the channels in the open state is the absence of energy barrier at the intracellular entrance of the vestibular cavity. There are nonetheless important variations regarding the overall stability of a cation as it approaches the center of the vestibular cavity (near $Z=0$) among the different channels. For example, the free energy is −4.3 kcal/mol for MthK, −6.1 kcal/mol for KvAP, and −4.9 kcal/mol for Shaker. In comparison, the corresponding free energy are 7.6 kcal/mol and −1.4 kcal/mol for the open state model I and II of KcsA, respectively. It is instructive to understand the origin of such differences from the results of Table 4. In particular, the open state model I of KcsA was generated directly from the backbone coordinates of the MthK channel. Hence, a comparison in this case can serve to highlight the influence of the amino acid sequence. In model I of KcsA, the unfavorable reaction field energy of an ion at the center of the cavity is larger (6.7 kcal/mol) than for MthK (2.0 kcal/mol). As shown in Figure 3, this is caused by the larger size of the side-chain residues, which makes the cavity slightly narrower. The static field contribution from the pore helices of MthK is smaller (−4.4 kcal/mol) than that of model I of KcsA (−7.0 kcal/mol), though the presence of charged residues near the cavity (Glu92, Arg93 and Glu96) further stabilizes a cation in the cavity. It follows that a cation is stable in the open vestibular cavity in the case of the MthK channel, but not in a model of KcsA constructed on the basis of the same backbone conformation (Figure 12).

Similarly, a comparison of open state model II of KcsA with the results for KvAP reveals also the importance of the amino acid sequence. In this case, the unfavorable reaction field energy from both structure are similar (1.7 kcal/mol for KvAP and 2.4 kcal/mol for model II of KcsA). The contribution from the pore helices is also similar (−6.0 kcal/mol for KvAP and −7.1 kcal/mol for model II of KcsA). The origin of the difference between KvAP and model II of KcsA is the presence of positively charged residues in TM2 of KcsA, which are responsible for destabilizing the ion in the cavity. Again, a cation is stable in the open vestibular cavity of KvAP, but not in model II of KcsA, which was constructed on the basis of the same backbone conformation. The difference between the results for model I and II of the open state of KcsA does not reflect on the uncertainty of these models, but rather point to the influence of the geometry of the inner vestibule on the energetics of ion permeation.

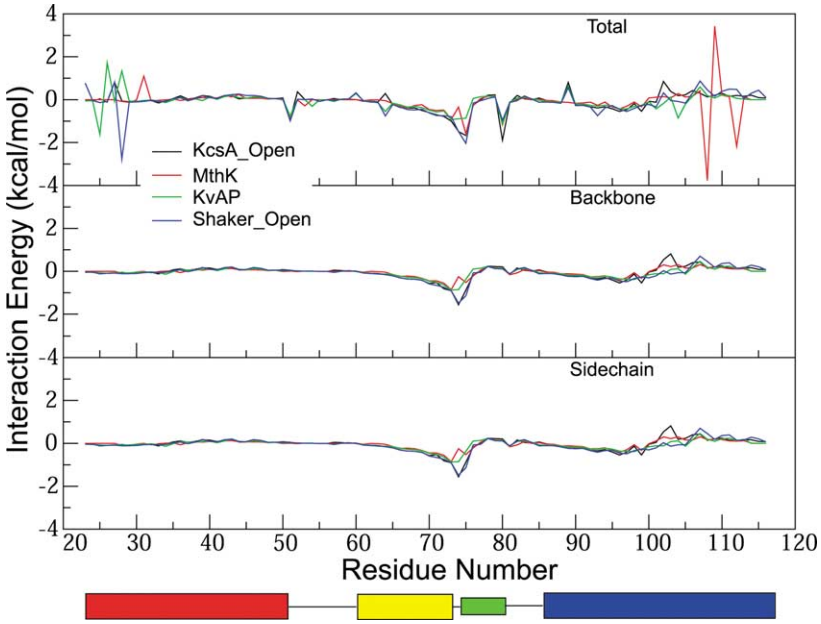

Figure 12. Static field energy where the interaction between the cavity ion and individual residues is calculated for all open channels. All the channels are aligned according to KcsA (the gaps are assigned a value of zero). The general topology of K^+ channels is given at the bottom of the Figure.

In the case of open state Shaker, the unfavorable reaction field energy at the center of the cavity (2.2 kcal/mol) is compensated by the favorable contribution from the pore helices (−8.0 kcal/mol), which gives rise to a net favorable energy for the open state (−4.9 kcal/mol). The static field energy from the pore helices is slightly larger because of the smaller opening of the intracellular gate as shown in Figure 3 (the static field tends to increase as the intracellular pore radius decreases). In addition, the presence of charged residues near the cavity increases the stability further. However, one should keep in mind that in the case of the 6-TM Shaker channel, the existence of aqueous regions associated with the voltage sensor (TM segments 1 to 4) could alter the electrostatic properties affecting the stability of a cation in the central cavity of the pore domain. The presence of high dielectric medium surrounding some region of the pore domain should tend to decrease the differences in electrostatic properties between the open and closed state. In the case of two TM channels such as KcsA, MthK, and KirBac1.1, representing the environment surrounding the pore domain, as a low dielectric lipid is less uncertain. For comparison, the stabilization of a K^+ located at the center of the cavity of the Kv1.2 channel is −5.3 kcal/mol, which is very similar to the value in KvAP (−6.1 kcal/mol).

In the KirBac1.1 channel, two glutamic acid residues, Glu106 and Glu130, might have a critical influence on the energy of ion in the cavity. To estimate the relative stability of the protonated and unprotonated states of ionizable side-chains in the complex dielectric environment, continuum electrostatic calculations can be used.[10,41,42] According to the calculations, a protonated state of Glu130 is stabilized by −21 kcal/mol relative to the unprotonated state. Although the continuum electrostatic result is most certainly an overestimate, it suggests that Glu130 side-chain should be protonated under normal conditions at pH 7. This value is obtained assuming that the three other Glu130 residues are protonated and that ions are present in the channel, i.e. with the most destabilizing conditions for proton binding. The Glu130 from the different subunits and the cation in the cavity are not strongly coupled and the calculated pK_a is essentially unchanged whether or not there is a cation in the cavity and the Glu130 side-chains of the three other monomers are unprotonated. Upon close observation of the structure of KirBac1.1, the Glu130 side-chains are embedded in the core of the protein and are far away from each other and also from the selectivity filter.

Functional implications

The present continuum electrostatic computations indicate that increasing the width of the intracellular entryway has two consequences on the energy of an incoming cation: (1) the unfavorable reaction field becomes smaller; and (2) the favorable static field from the pore helices also becomes smaller. The decrease in the unfavorable reaction field is, of course, entirely expected as the aqueous cavity becomes contiguous with the high dielectric intracellular solution. On the other hand, the decrease in the favorable static field from the pore helices is slightly more unexpected (though it makes sense, in retrospect). Additional factors associated with the magnitude of the entrance barrier appear to be less important: Figure 7 shows that the barrier becomes rapidly negligible as soon as the vestibular entrance to the channel reaches a sufficient width. The resulting free energy of transfer of a cation inside the vestibular cavity of an open channel can be significantly modulated by

the presence of charged residues associated with the inner helices. The energy of a cation in the cavity of MthK would decrease from −4.3 kcal/mol to −1.0 kcal/mol upon cancellation of the charges on residues Glu92, Arg93 and Glu96 at the COO terminus of TM2. In contrast, the presence of positive charges at the end of the TM2 in KcsA destabilize an ion in the cavity by 2.5 kcal/mol. The favorable energy in the case of Shaker is attributed to the presence of charged residues Glu395 and Glu418, which contributes an extra −11 kcal/mol in the closed state and −3.8 kcal/mol in the open state. In the case of Shaker, KvAP (and Kv1.2), the presence of charged residues on the extracellular loops has also some stabilizing effect.

These purely electrostatic factors could have a significant impact on the functional properties of biological channels. Typically, a cation at the center of the cavity is less stable in the open state than in the closed state. The difference in affinity might have some functional utility, for example, to protect the integrity of the structure by insuring that a K^+ binds in the cavity upon channel closing. Furthermore, all K^+ channels are obviously not expected to have identical intracellular vestibular entrance (e.g. MthK and KvAP). A calcium-activated channel like MthK displays a very wide opening (15 Å), whereas a voltage-activated channel like KvAP has a slightly narrower, but still large, opening (12 Å). The present analysis suggests that the intracellular opening of the pH-activated KcsA channel is closer to that of KvAP than of MthK. It is possible that the gating machinery controlling the intracellular gate formed by the helical bundle requires different molecular geometries of the vestibular entrance to these different channels. Detailed structural information about eukaryotic ligand-gated channels, or calcium–calmodulin-gated channels is presently lacking, but it may be anticipated that each mechanism imposes specific structural constraints on the width and shape of the open gate. Variations in the geometry of the pore entrance, in turn, give rise to electrostatic constraints on ion permeation and, thus, have important functional consequences on K^+ channels. Under physiological conditions, the concentration of permeant ions C and the transmembrane potential are tightly regulated and the amount of ionic current going through a given membrane can be modulated *via* the total number of active channels (synthesis), their open probability (gating), or their unitary conductance (permeation). What are the factors affecting the unitary conductance g? At the simplest level, the latter can be expressed as $g = g_{max} K_b C/(1 + K_b C)$, where g_{max} is the maximum conductance corresponding to the ultimate turnover of ion transport by the pore under saturating conditions, and K_b is an effective (semi-equilibrium) binding constant K_b (a simple first-order form applies also to a multi-ion channel such as KcsA).[47] The maximum conductance of K^+ channels is roughly in the range of 300 ps–500 ps, near the diffusion limit. It is intimately related to the structural and dynamical properties of the highly conserved selectivity filter, which cannot be increased in any obvious way without altering ion selectivity as well. Increasing the unitary conductance by increasing the effective association constant K_b is, on the other hand, much easier. This suggests that, once the geometry of the intracellular channel entrance is set (by the molecular machinery for activating the gate for example), the loss of favorable static field interactions from the pore helices could be offset by the introduction of a few charged residues near the COO terminus of the inner helices. This could explain, in particular, why the sequence of MthK is such that a cation is electrostatically stabilized in this wide-open cavity, whereas it is not so when the sequence of KcsA is mapped onto this same geometry.

It is well known that the presence of charged residues "decorating" the intracellular entryway of K^+ channels has important functional consequences.[1] For example, Magleby *et al.*[48] and Miller *et al.*[49] showed that the unusually large conductance of the Ca^{2+} and voltage-activated K^+ channels (BK) is related to the presence of negatively charged residues in the vestibule region; there is a ring of eight conserved negatively charged amino acid residues at the inner vestibule. BK channels are found in neurons, striated and smooth muscle, endocrine and exocrine glands, and kidney tubules. Their main role is to link cell metabolism to membrane conductance. For example, in renal collecting ducts, members of the BK family (MaxiK) provide passive transport pathway from the cell to the lumen and a large conductance is required for large efflux of K^+. Similarly, differences between two closely related inwardly rectifying channels, Kir1.1 and Kir2.1, found, respectively, in the kidney and in smooth muscle, can be understood.[1] The only major difference between these two channels, which display a twofold change in their conductance, is the presence of neutral or charged residues near the intracellular entry.[50] In Kir2.1, which is found in the skeletal muscle where a low throughput is required, there are arginine residues near the entry pathway. In Kir1.1, which is found in the kidney where a high throughput is required, those arginine residues are replaced by neutral glutamine residues yielding a two-fold increase in the channel conductance.[50] In the case of KcsA, it has been shown that mutating a neutral residue (Ala108) to a negatively charged residue (Asp) in the vestibule increases the channel conductance;[49] a simple PB calculation indicates that a cation in the cavity would be further stabilized by −3.3 kcal/mol for the open state of this mutant. Hence, both the geometry and charge distribution of the inner vestibule have an impact on the functional properties of the various K^+ channels and this may have affected their evolution.

Summary

Poisson–Boltzmann calculations were used to examine the electrostatic properties of the vestibular cavity on the intracellular side of K^+ channels. In the closed state KcsA based on the crystallographic structure of the channel, more than 80% of the total electrostatic free energy comes from the pore helices, whereas in various models of the KcsA channel in the open state, the static field from the pore helices is significantly decreased. The total stabilization from the pore helices is about -27 kcal/mol in the closed state compared to -7 kcal/mol in the open state. Despite their slightly different orientation, the pore helices in KirBac1.1 also contribute to stabilize a cation in the cavity at least as well as in the KcsA channel. Analysis of the electrostatic properties of intermediate models of KcsA generated using a linear interpolation scheme suggests that the optimal pore opening for KcsA is roughly 9 Å. This is smaller than the opening in the X-ray structure of the MthK channel, but rather similar to the open in the X-ray structure of the KvAP channel. All the "closed state" channels are characterized by a large energy barrier at the entrance of the pore, near the narrow helical bundle crossing at the intracellular side arising from the reaction field energy (corresponding to a dehydration penalty). Similarly, all the "open state" channels are characterized by the absence of energy barrier at the intracellular entrance of the vestibular cavity. Nonetheless, differences in the geometry of the vestibular cavity as well as the presence of charged amino acid along the inner helices can give rise to important variations in the electrostatic properties among the open state channels. For example, a cation can be more stable in the cavity of the MthK or the KvAP channels than in open state models of KcsA constructed with the same backbone conformation. Therefore, the amino acid sequence near the inner entry pathway can have an important impact on the overall permeation properties of K^+ channels. Purely electrostatic factors give rise to energetic constraints that have important functional consequences on the various K^+ channels, and partly explain the presence or absence of charged residues near the inner vestibular entry. It will be of interest to examine how the electrostatic properties of the intracellular vestibules of K^+ channels is affecting the diffusional access resistance using Brownian dynamics simulations.[51]

References

1. Hille, B. (2001). *Ionic Channels of Excitable Membranes.* 3rd edit, Sinauer, Sunderland, MA.
2. Doyle, D., Cabral, J., Pfuetzner, R., Kuo, A., Gulbis, J., Cohen, S. *et al*. (1998). The structure of the potassium channel: molecular basis of K^+ conduction and selectivity. *Science*, **280**, 69–77.
3. Heginbotham, L., Abramson, T. & MacKinnon, R. (1992). A functional connection between the pores of distantly related ion channels as revealed by mutant K^+ channels. *Science*, **258**, 1152.
4. Zhou, Y. & MacKinnon, R. (2004). Ion binding affinity in the cavity of the KcsA potassium channel. *Biochemistry*, **43**, 4978–4982.
5. Roux, B. & MacKinnon, R. (1999). The cavity and pore helices in the KcsA K^+ channel: electrostatic stabilization of monovalent cations. *Science*, **285**, 100–102.
6. Chakrabarti, N., Roux, B. & Pomes, R. (2004). Molecular basis of proton blockage in aquaporins. *J. Mol. Biol.* **343**, 493–510.
7. Dutzler, R., Campbell, E., Cadene, M., Chait, B. & MacKinnon, R. (2002). X-ray structure of a ClC chloride channel at 3.0 Å reveals the molecular basis of anion selectivity. *Nature*, **415**, 287–294.
8. Dutzler, R., Campbell, E. & MacKinnon, R. (2003). Gating the selectivity filter in ClC chloride channels. *Science*, **300**, 108–112.
9. Bernèche, S. & Roux, B. (2000). Molecular dynamics of the KcsA K(+) channel in a bilayer membrane. *Biophys. J.* **78**, 2900–2917.
10. Roux, B., Bernèche, S. & Im, W. (2000). Ion channels, permeation and electrostatics: insight into the function of KcsA. *Biochemistry*, **39**, 13295–13306.
11. Cuello, L. G., Romero, J. G., Cortes, D. M. & Perozo, E. (1998). pH-dependent gating in the streptomyces lividans K^+ channel. *Biochemistry*, **37**, 3229–3236.
12. Perozo, E., Cortes, D. & Cuello, L. (1999). Structural rearrangements underlying K^+-channel activation gating. *Science*, **285**, 73–78.
13. Heginbotham, L., LeMasurier, M., Kolmakova-Partensky, L. & Miller, C. (1999). Single streptomyces lividans K(+) channels. Functional asymmetries and sidedness of proton activation. *J. Gen. Physiol.* **114**, 551–560.
14. Zhou, Y., Morais-Cabral, J. H., Kaufman, A. & MacKinnon, R. (2001). Chemistry of ion coordination and hydration revealed by a K^+ channel-Fab complex at 2.0 Å resolution. *Nature*, **414**, 43–48.
15. Jiang, Y., Lee, A., Chen, J., Cadene, M., Chait, B. T. & MacKinnon, R. (2002). Crystal structure and mechanism of a calcium-gated potassium channel. *Nature*, **417**, 515–522.
16. Cortes, D., Cuello, L. & Perozo, E. (2001). Molecular architecture of full-length KcsA: role of cytoplasmic domains in ion permeation and activation gating. *J. Gen. Physiol.* **117**, 165–180.
17. Kelly, B. L. & Gross, A. (2003). Potassium channel gating observed with site-directed mass tagging. *Nature Struct. Biol.* **10**, 280–284.
18. Kuo, A., Gulbis, J. M., Antcliff, J. F., Rahman, T., Lowe, E. D., Zimmer, J. *et al*. (2003). Crystal structure of the potassium channel KirBac1.1 in the closed state. *Science*, **300**, 1922–1926.
19. Jiang, Y., Lee, A., Chen, J., Ruta, V., Cadene, M., Chait, B. & MacKinnon, R. (2003). X-ray structure of a voltage-dependent K^+ channel. *Nature*, **423**, 33–41.
20. Li, W. & Aldrich, R. (2004). Unique inner pore properties of BK channels revealed by quarternary ammonium block. *J. Gen. Physiol.* **124**, 43–57.
21. Liu, Y., Holmgren, M., Jurman, M. & Yellen, G. (1997). Gated access to the pore of a voltage-dependent K^+ channel. *Neuron*, **19**, 175–184.
22. Holmgren, M., Shin, K. S. & Yellen, G. (1998). The activation gate of a voltage-gated K^+ channel can be trapped in the open state by an intersubunit metal bridge. *Neuron*, **21**, 617–621.

23. del Camino, D., Holmgren, M., Liu, Y. & Yellen, G. (2000). Blocker protection in the pore of a voltage-gated K^+ channel and its structural implications. *Nature*, **403**, 321–335.
24. Bruhova, I. & Zhorov, B.S. (2005). KvAP-based model of the pore region of Shaker potassium channel is consistent with cadmium- and ligand-binding experiments. *Biophys. J.* **89**, 1020–1029.
25. Long, S., Campbell, E.B. & Mackinnon, R. Crystal structure of a mammalian voltage-dependent Shaker family K^+ channel. *Science*.
26. Honig, B. & Nicholls, A. (1995). Classical electrostatics in biology and chemistry. *Science*, **268**, 1144.
27. Gilson, M. & Honig, B. (1986). The dielectric constant of a folded protein. *Biopol.* **25**, 2097–2119.
28. Warwicker, J. & Watson, H. (1982). Calculation of the electric potential in the active site cleft due to alpha-helix dipoles. *J. Mol. Biol.* **157**, 671–679.
29. Im, W., Beglov, D. & Roux, B. (1998). Continuum salvation model: computation of electrostatic forces from numerical solutions to Poisson–Boltzmann equation. *Comp. Phys. Commun.* **111**, 59–75.
30. Brooks, B., Bruccoleri, R., Olafson, B., States, D., Swaminathan, S. & Karplus, M. (1983). CHARMM: a program for macromolecular energy minimization and dynamics calculations. *J. Comput. Chem.* **4**, 187–217.
31. Bernèche, S. & Roux, B. (2002). The ionization state and the conformation of Glu-71in the KcsA K(+) channel. *Biophys. J.* **82**, 772–780.
32. Bower, M., Cohen, F. & Dunbrack, R. (1997). Prediction of protein side-chain rotamers from a backbonedependent rotamer library: a new homology modeling tool. *J. Mol. Biol.* **267**, 1268–1282.
33. White, S. & Wiener, M. (1996). The liquid crystallographyc structure of fluid lipid bilayer membranes. In *Biological Membranes. A Molecular Perspective from Computation and Experiment* (Merz, K & Roux, B., eds), pp. 127–144, Birkhauser, Boston.
34. Nina, M., Beglov, D. & Roux, B. (1997). Atomic radii for continuum electrostatics calculations based on molecular dynamics free energy simulations. *J. Phys. Chem. B*, **101**, 5239–5248.
35. Roux, B. (1997). The influence of the membrane potential on the free energy of an intrinsic protein. *Biophys. J.* **73**, 2980–2989.
36. MacKerell, A. J., Bashford, D., Bellot, M., Dunbrack, R., Evanseck, J. & Field, M. (1998). All-atom empirical potential for molecular modeling and dynamics studies of proteins. *J. Phys. Chem. B*, **102**, 3586–3616.
37. Simonson, T. & Perahia, D. (1995). Microscopic dielectric properties of cytochrome c from molecular dynamics simulations in aqueous solution. *J. Am. Chem. Soc.* **117**, 7987–8000.
38. King, G., Lee, F. & Warshel, A. (1991). Microscopic simulation of macroscopic dielectric constants of solvated proteins. *J. Chem. Phys.* **95**, 4365–4377.
39. Simonson, T. & Brooks, C. L., III (1996). Charge screening and the dielectric constant of proteins: insights from molecular dynamics. *J. Am. Chem. Soc.* **118**, 8452–8458.
40. Warshel, A. & Russell, S. T. (1984). Calculations of electrostatic interactions in biological systems and in solutions. *Quart. Rev. Biophys.* **17**, 283–422.
41. Bashford, D. & Karplus, M. (1990). pK_a's of ionizable groups in proteins: atomic detail from a continuum electrostatic model. *Biochemistry*, **29**, 10219–10225.
42. Antosiewicz, J., McCammon, J. & Gilson, M. (1996). The determinants of pK_as in proteins. *Biochemistry*, **35**, 7819–7833.
43. Beckstein, O., Tai, K. & Sansom, M. (2004). Not ions alone: barriers to ion permeation in nanopores and channels. *J. Am. Chem. Soc.* **126**, 14694–14695.
44. Liu, Y., Sompornpisut, P. & Perozo, E. (2001). Structure of the KcsA channel intracellular gate in the open state. *Nature Struct. Biol.* **8**, 883–887.
45. Zhou, M., Morais-Cabral, J. H., Mann, S. & MacKinnon, R. (2001). Potassium channel receptor site for the inactivation gate and quaternary amine inhibitors. *Nature*, **411**, 657–661.
46. Faraldo-Gomez, J. D. & Roux, B. (2004). Electrostatics of ion stabilization in a ClC chloride channel homologue from *Escherichia coli*. *J. Mol. Biol.* **339**, 981–1000.
47. Bernèche, S. & Roux, B. (2003). A microscopic view of ion conduction through the kcsa K^+ channel. *Proc. Natl Acad. Sci.* **100**, 8644–8648.
48. Brelidze, T. I., Niu, X. & Magleby, K. L. (2003). A ring of eight conserved negatively charged amino acids doubles the conductance of BK channels and prevents inward rectification. *Proc. Natl Acad. Sci. USA*, **100**, 9017–9022.
49. Nimigean, C., Chappie, J. & Miller, C. (2003). Electrostatic tuning of ion conductance in potassium channels. *Biochemistry*, **42**, 9263–9268.
50. Zhang, Y., Robertson, J., Gray, D. & Palmer, L. (2004). Carboxy-terminal determinants of conductance in inward-rectifier K channels. *J. Gen. Physiol.* **124**, 729–739.
51. Im, W., Seefeld, S. & Roux, B. (2000). A grand canonical Monte Carlo—Brownian dynamics algorithm for simulating ion channels. *Biophys. J.* **79**, 788–801.
52. Thompson, J., Higgins, D. & Gibson, T. (1994). CLUSTAL W: improving the sensitivity of progressive multiple sequence alignment through sequence weighting, position-specific gap penalties and weight matrix choice. *Nucl. Acids Res.* **22**, 4673–4680.

Edited by G. von Heijne

(Received 10 June 2005; received in revised form 9 September 2005; accepted 10 September 2005)
Available online 30 September 2005